Geochemistry Geophysics Geosystems G3
AN ELECTRONIC JOURNAL OF THE EARTH SCIENCES
Published by AGU and the Geochemical Society

Article
Volume 6, Number 3
30 March 2005
Q03012, doi:10.1029/2004GC000821
ISSN: 1525-2027

Effects of normal stress perturbations on the frictional properties of simulated faults

Tiancong Hong and Chris Marone
Department of Geosciences, Pennsylvania State University, 536 Deike Building, University Park, Pennsylvania 16802, USA (cjm38@psu.edu)

[1] We report on laboratory experiments to investigate the frictional response of creeping faults to sudden changes in normal stress. Experiments were conducted on layers of quartz powder, bare surfaces of Westerly granite, and layers of a 50/50 mixture of quartz powder and smectite clay powder. The tests were carried out at room temperature and controlled humidity using a servo-controlled double-direct shear configuration. Normal stress perturbations, corresponding to loading and unloading of tectonic fault zones, were applied during steady sliding at constant loading rate from 3 to 1000 μm/s (shear strain rates of 1.5×10^{-3} to 0.5 s^{-1}). Sudden changes in normal stress resulted in a linear elastic response of shear stress followed by a transient evolution of friction over a characteristic displacement. The transient, inelastic response is quantified as $\alpha = (\Delta\tau_\alpha/\sigma)/\ln(\sigma/\sigma_0)$, where $\Delta\tau_\alpha$ is the transient change in shear stress following a step change from initial normal stress σ_0 to final normal stress σ. We find that α is independent of sliding velocity and varies with ambient relative humidity and shear loading history. For unloading, we document a transition from stable to unstable behavior as a function of net slip in the range 3 to 30 mm (shear strains of 1.5 to 15). Increased humidity led to higher values of α for pure quartz gouge, but smaller α for the quartz-clay gouge. The effects of shear displacement and humidity are discussed in the context of particle characteristics and gouge fabric development. The extended rate- and state-dependent friction laws, using one state variable and the Ruina evolution law with normal stress variation, describe our observations.

Components: 9324 words, 15 figures, 1 table.

Keywords: faulting; friction; stability.

Index Terms: 3902 Mineral Physics: Creep and deformation; 5104 Physical Properties of Rocks: Fracture and flow; 7209 Seismology: Earthquake dynamics (1242).

Received 23 August 2004; **Revised** 20 January 2005; **Accepted** 9 February 2005; **Published** 30 March 2005.

Hong, T., and C. Marone (2005), Effects of normal stress perturbations on the frictional properties of simulated faults, *Geochem. Geophys. Geosyst.*, *6*, Q03012, doi:10.1029/2004GC000821.

1. Introduction

[2] Understanding the effects of dynamic stressing on fault zone strength and stability is a central problem in studies of fault interaction and earthquake triggering. Earthquakes alter the stress field in the vicinity of their ruptures and emit seismic waves that influence the stress field thousands of kilometers away. Recent work shows that large earthquakes can increase seismicity rates both near [*Gomberg et al.*, 1997; *Wyss and Wiemer*, 2000; *Kilb et al.*, 2000, 2002] and far from the fault rupture [*Gomberg and Bodin*, 1994; *Spudich et al.*, 1995; *Gomberg*, 1996; *Gomberg and Davis*, 1996; *Harris*, 1998] as well as trigger tectonic earthquakes [*Hill et al.*, 1993; *Gomberg et al.*, 1997].

[3] Tectonic fault zones are subject to variations in normal stress on a wide range of spatiotemporal scales. In addition to the stress changes caused by earthquakes, many other sources may also alter fault zone stresses. Periodic stressing from ocean

and Earth tides alter the subsurface stress field and can affect seismicity rates [*Perfettini and Schmittbuhl*, 2001; *Wilcock*, 2001; *Tolstoy et al.*, 2002; *Vidale et al.*, 1998]. Variations in fault properties can also induce nonuniform slip, which in turn results in spatial and temporal variations in fault normal stress [*Cochard and Rice*, 2000; *Ranjith and Rice*, 2001]. Other factors, such as fault roughness and wave reflections from the free surface can also contribute to variations of normal stress [*Harris and Day*, 1993; *Bouchon and Streiff*, 1997; *Oglesby et al.*, 1998].

[4] Effects of dynamic stressing on frictional strength and stability changes have been investigated by numerical simulations and laboratory studies. *Richardson and Marone* [1999] found that both healing and relaxation of granular shear zones are enhanced by normal stress oscillations. *Bureau et al.* [2000] and *Cochard et al.* [2003] studied the effect of high frequency normal load vibrations and found that even a modest modulation induced substantial frictional weakening. *Tworzydlo and Hamzeh* [1997] noted that the inclusion of normal force vibrations in models of rock friction can cause instability. Theoretically, *Perfettini et al.* [2001] identified a resonant response of shear zone strength, involving strong amplification of the shear stress and velocity response for a small range of friction parameters and a critical loading stiffness. In the laboratory, *Boettcher and Marone* [2004] found that periodic normal-force vibrations weaken and potentially destabilize steadily creeping fault zones.

[5] It is well known that sudden decreases in normal stress can destabilize slip [*Simões and Martins*, 1998; *Cochard and Rice*, 2000; *Ranjith and Rice*, 2001; *Ben-Zion*, 2001] and recent studies of the effect of normal stress on fault strength and stability have drawn increasing attention [*Olsson*, 1988; *Linker and Dieterich*, 1992; *Wang and Scholz*, 1994; *Prakash and Clifton*, 1993; *Prakash*, 1998; *Richardson and Marone*, 1999]. *Linker and Dieterich* [1992] studied friction of bare Westerly granite and showed that a step increase in normal stress has an immediate effect followed by a memory-like transient evolution in frictional strength with continuing slip or time to a new steady state. This observation was confirmed by the works of *Wang and Scholz* [1994] on bare Westerly granite and *Richardson and Marone* [1999] on gouge layers of fine-grained quartz powder. *Linker and Dieterich* [1992] interpreted their observations by extending the rate/state frictional laws to incorporate a new parameter α, which describes the evolution of frictional strength following a step change in normal stress.

[6] Theoretical work shows that α should be in the range: $0 \leq \alpha \leq \mu_{ss}$ [*Perfettini et al.*, 2001], where μ_{ss} is the coefficient of sliding friction. Measured values of α on geological materials at sliding velocities of order 1–10 μm/s are in the range 1/3 to 1/2 of μ_{ss} [*Linker and Dieterich*, 1992; *Richardson and Marone*, 1999]. However, experiments involving oblique shock impact on hard metal at sliding velocities of order 10 m/s indicate that α approaches μ_{ss} [*Prakash and Clifton*, 1993; *Prakash*, 1998]. The discrepancy is significant, since resonant conditions and the potential for fault instability depend critically on α. At present it is difficult to explain the discrepancy in reported values of α, because of the paucity of available laboratory data. The work by Prakash and colleagues has been performed on metals at high velocity and with only unloading perturbations in normal stress at very high ambient stresses. Their experiments exhibit only gradual evolution in shear stress in response to a step change in normal stress. The work on geologic materials has been conducted at lower normal stress, lower velocity, and with a focus on increases in normal stress [*Linker and Dieterich*, 1992; *Richardson and Marone*, 1999]. To our knowledge, there are no existing laboratory data on the effects of sliding velocity or normal stress perturbation sign (loading/unloading) on α.

[7] The purpose of this paper is to report results from a detailed laboratory study of normal-stress stepping experiments (both increases and decreases) during steady shear loading over a wide range of conditions. We found that α differs for loading and unloading normal stress perturbations and that it varies with frictional material, ambient humidity, and net shear strain. Our results do not fully resolve discrepancies with existing measurements of α; however, the particle-based interpretations of our results provide important guidance for understanding these differences and for applying the laboratory results to tectonic faults.

2. Laboratory Technique

2.1. Apparatus and Sample

[8] Our experiments were performed in a servo-controlled biaxial loading apparatus at room temperature and controlled humidity using the

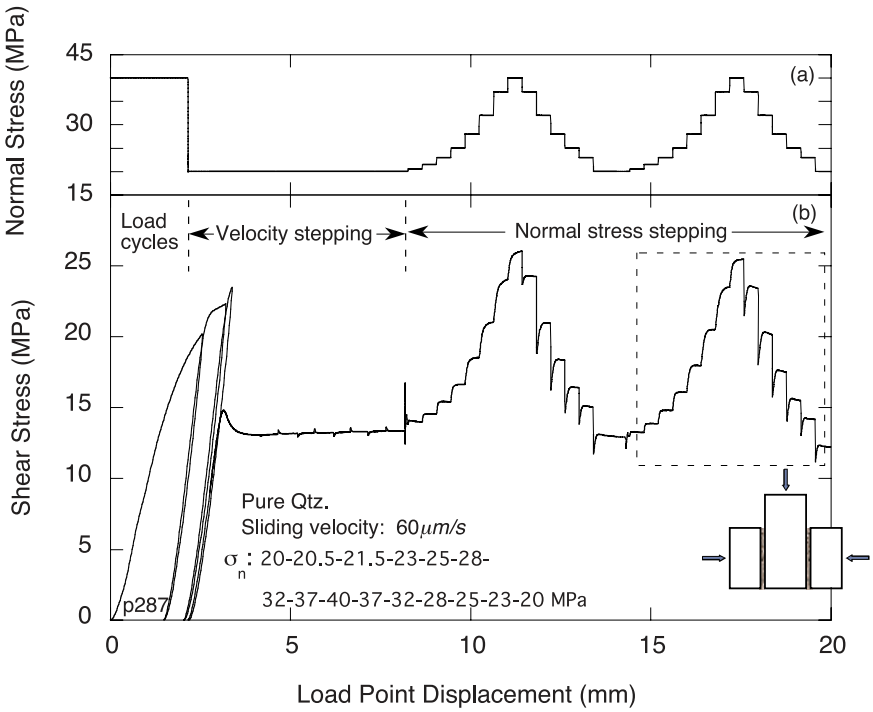

Figure 1. (a) Imposed normal stress history and (b) shear stress response versus load point displacement for an entire experiment. Two layers of quartz gouge were sheared at a loading rate of 60 μm/s. Layers were preconditioned by conducting 3 load cycles and a series of velocity steps. Normal stress changes are instantaneous and occur during steady creep at constant shear loading rate. Normal stress history is listed in Figure 1b. Detail for the shear response (dashed box) is shown in Figure 2a. Inset illustrates the double-direct shear configuration.

double-direct shear geometry (Figure 1 inset). The apparatus consists of two separate hydraulic loading rams in vertical and horizontal directions, respectively. In this configuration, two frictional surfaces are sheared simultaneously between three blocks. The vertical ram drives the central block in displacement feedback mode with 0.1 μm resolution. The horizontal ram applies normal stress in load feedback mode with 0.1 kN resolution. Displacement and forces were measured by displacement transducers (DCDTs) and load cells mounted on the rams at the load point position. The machine stiffness for the vertical load frame is 5 MN/cm. The displacement on the frictional surfaces was calculated using the calibrated stiffness from the load point. The position and applied force of each ram are recorded continuously at 10 kHz and averaged to sampling rates between 1 and 1000 Hz. Additional details about the apparatus are given by *Mair and Marone* [1999] and *Frye and Marone* [2002].

[9] Layers of simulated fault gouge were constructed in a leveling jig to be precisely 3 mm thick. Layers were sheared between grooved steel forcing blocks fitted with guide plates to inhibit gouge loss along the layer edges. The side forcing blocks were $10 \times 10 \times 2$ cm^3 and the center block was $10 \times 15 \times 3$ cm^3. A constant nominal frictional contact area of 10×10 cm^2 was maintained throughout shear. Roughened surfaces were triangular grooves 0.8 mm deep and 1 mm wavelength cut perpendicular to the shear direction. These promote a transition from distributed, pervasive shear to progressively localized shear as a function of increasing net strain. Shear strain is calculated as the sum of incremental shear displacement divided by the instantaneous layer thickness.

[10] The quartz powder is subangular Ottawa sand (>99% S_iO_2), obtained as Natural Grain product F-110 from the U.S. Silica Co. The median particle size is 110 μm and particles are initially 50 to 150 μm in diameter. Grinding during shear reduces the smallest particles to 1–10 μm. We also studied gouge composed of a mixture of the quartz powder and smectite clay powder in the proportion 50% versus 50% by weight. Commercially obtained smectite clay is a Ca-smectite powder with grain size in the range of 2–500 μm (see *Saffer et al.* [2001] for additional details).

Table 1. Experimental Details

Experiment	Sliding Rate, μm/s	Material	Humidity, %
p193, p196	10	quartz	49
p276, p280	30	quartz	51
p287, p288	60	quartz	45
p290, p305	100	quartz	35
p306, p312	300	quartz	40
p315	3	quartz	45
p316, p317	600	quartz	42
p318	1000	quartz	42
p324	1000	quartz	19
p325	30	Westerly	16
p357	100	clay-quartz	42
p363	300	clay-quartz	20
p373	60	clay-quartz	25
p380	30	clay-quartz	40
p385	600	clay-quartz	40
p386	10	clay-quartz	40
p400	3	clay-quartz	33
p401	1000	clay-quartz	32
p411	10	quartz	8
p418, p421	30	quartz	9
p430	30	quartz	11
p432	30	clay-quartz	19
p434, p439	30	clay-quartz	13
p443	30	clay-quartz	14
p445	30	Westerly	22

[11] Experiments were also performed on Westerly granite blocks without gouge. The surfaces of Westerly granite were ground flat and smooth, then sand-blasted to increase roughness. The granite blocks had a constant nominal area of contact of 95.2×99.1 mm^2.

2.2. Experimental Procedure

[12] The shear and normal loading history were controlled by a digital, external signal and were identical from one experiment to the next. Step changes in normal stress were accomplished in <0.01 s. The total slip at each normal stress level was set to 400 μm, which was sufficient for the shear stress to reach a new steady state. Normal stress was defined in the range of 10–45 MPa in tests on gouge layers and 5–12 MPa in tests on granite blocks. The magnitude of step changes ranged from 0.5 to 6 MPa. Changes of normal stress resulted in Poisson expansion of the center block and thus an increase in applied shear load. We carried out calibrations of the testing machine and made corrections for this effect.

[13] Experiments began with three cycles of shear loading and unloading under a normal stress of 40 MPa (Figure 1). These were carried out to produce new surface area in situ within the gouge [e.g., *Frye and Marone*, 2002]. After the load cycles, we performed velocity stepping tests (between 10 and 100 μm/s) under a constant normal stress of 20 MPa. The shear loading cycles and net shear strain during velocity stepping promote development of a steady state particle size distribution and fabric within the fault gouge. Typically, the sliding system changed from velocity strengthening frictional behavior, in which the steady state coefficient of sliding friction increases with velocity, to velocity weakening frictional behavior after the load cycles and velocity steps. Normal stress stepping tests were then conducted by repeating a sequence of normal stress segments (Figure 1). To study the effect of net displacement, a different procedure was used in which normal stress stepping was conducted throughout the total displacement range, without load cycles and velocity steps. Experiment details are given in Table 1.

3. Data and Observations

[14] In Figure 1, we show the complete results of experiment p287 in which two sets of normal stress (σ) steps were imposed during steady shear loading of quartz gouge. The first and second set of positive stressing steps produced qualitatively similar behavior. Normal stress increases produced an elastic increase in shear stress and inelastic fric-

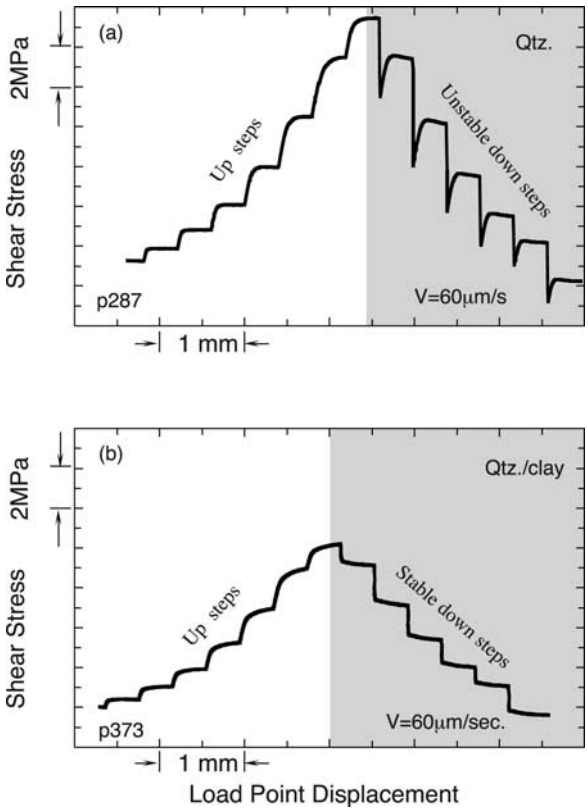

Figure 2. Shear stress responses of (a) pure quartz and (b) clay-quartz gouge for the same normal stress and shear loading history (see Figure 1). The materials behave similarly for normal stress increases; however, there are qualitative differences in the response to normal stress reduction. A step decrease in normal stress induces dynamic instability more easily for pure quartz gouge than for clay-quartz mixtures.

tional strengthening. Unloading steps resulted in an instantaneous stick-slip instability followed by stable sliding, and the degree of instability increased with net displacement (Figure 1). The second set of stress perturbations (dashed box) is shown in detail in Figure 2a. Upon a step increase in normal stress, shear stress exhibited a linear, elastic response followed by gradual strengthening to a new steady state level. Unloading steps resulted in stick-slip instability followed by strengthening. Layers of clay-rich gouge exhibited qualitatively similar behavior to that of pure quartz for loading steps; however, the magnitude of the shear strength increase was significantly smaller for the clay/quartz layers (Figure 2). Also, the clay-rich layers continued to shear stably and did not stick-slip upon unloading normal stress steps (Figure 2). These results are generally consistent with previous studies performed under similar conditions [*Linker and Dieterich*, 1992; *Wang and Scholz*, 1994; *Richardson and Marone*, 1999].

[15] Detailed measurements of the effect of normal stress changes on shear strength were carried out for each normal stress step (Figure 3). Figure 3 shows one stress increase from the initial normal stress σ_0 to final normal stress σ and the corresponding shear strength response. The parameter τ_{ss} is the steady state shear stress at σ. Following *Linker and Dieterich* [1992], we measure the elastic $\Delta\tau_e$ and transient, inelastic $\Delta\tau_\alpha$ parts of the shear stress response to a stress step (Figure 3). In addition, we measure the slip distance d_α over which shear strength evolves following a stress step and the total change in frictional strength $\Delta\tau_t = \Delta\tau_e + \Delta\tau_\alpha$. The point where shear loading deviates from linear elastic loading is defined as $\tau_{elastic}$. Following *Richardson and Marone* [1999], $\tau_{elastic}$ was determined by incre-

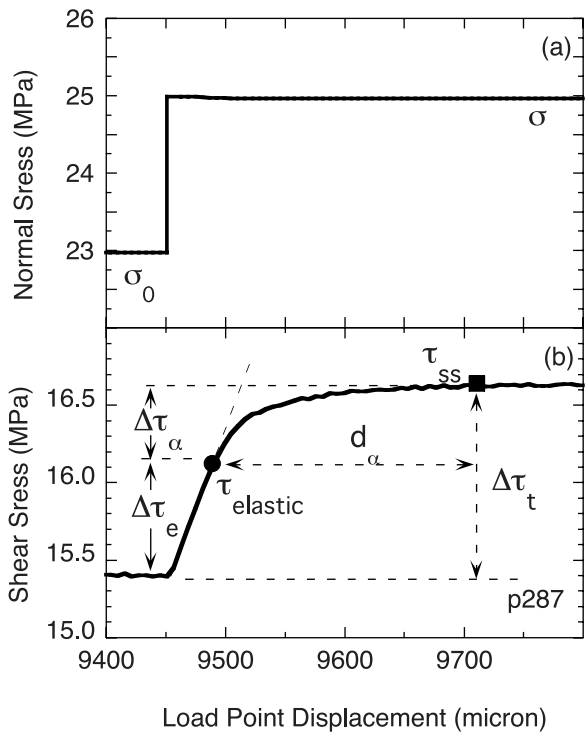

Figure 3. (a) Normal stress and (b) shear response versus load point displacement for one step increase from 23 to 25 MPa. In response to the step increase in normal stress, shear stress increases linearly along an elastic loading line until $\tau_{elastic}$ (marked with a solid circle), followed by a gradual evolution to a new steady state of τ_{ss} (marked with a solid square) over the displacement d_α. The difference $\Delta\tau_\alpha$ between $\tau_{elastic}$ and τ_{ss} is the evolutional change in shear stress, which determines α. Similarly, elastic change $\Delta\tau_e$ and total change $\Delta\tau_t$ in shear stress are defined as shown.

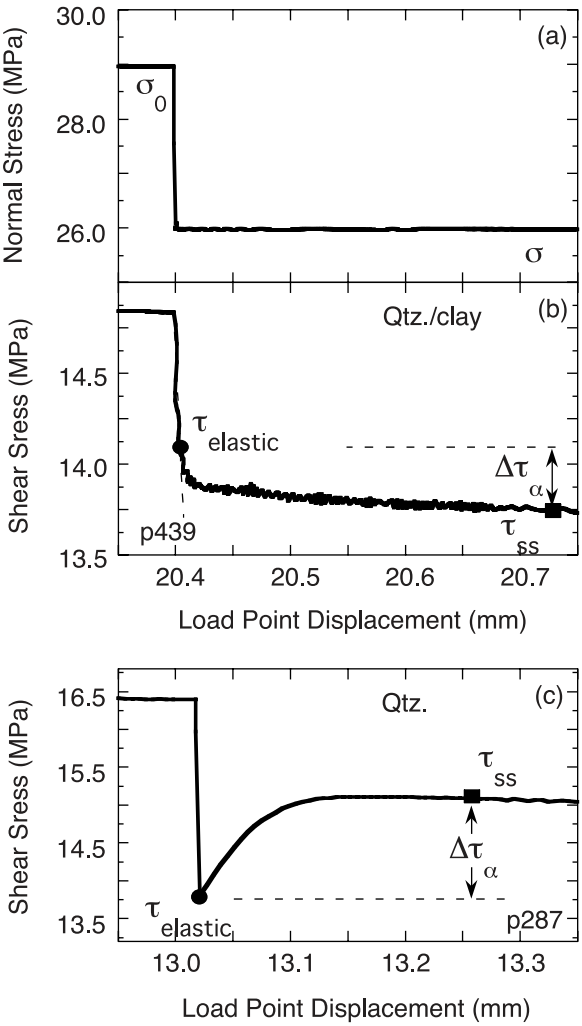

Figure 4. (a) Normal stress history for a step decrease from $\sigma_0 = 29$ to $\sigma = 26$ MPa. Shear strength response for (b) stable (clay-quartz) and (c) unstable (quartz) behavior. In both cases, shear stress decreases linearly along the elastic curve until $\tau_{elastic}$ and then evolves to a new steady state τ_{ss}. The sign of $\Delta\tau_\alpha$ is opposite for the two cases. The normal stress drop causes dynamic instability for quartz gouge.

mentally fitting a straight line in a least squares sense to the shear loading curve, beginning with the data point at the start of the normal stress step. One additional data point was added for each successive fit until the last local minimum in the error of fit was obtained. In this way, $\tau_{elastic}$ corresponds to the last data point with local minimum of error and defines an objective measure of the point at which the curve deviates from a straight line.

[16] Normal stress perturbations may result in a change in the residual coefficient of sliding friction $\mu_{ss} = \tau/\sigma_0$. If μ_{ss} remains constant for a normal stress step of magnitude $\Delta\sigma$, then $\Delta\tau_t/\Delta\sigma = \mu_{ss}$, and this in indeed the case in most of our tests. Our primary focus is on $\Delta\tau_\alpha$, which reflects the evolution in shear stress after a normal stress change. We measured $\Delta\tau_\alpha$ for both stable and unstable unloading steps in a similar way (Figure 4); however, due to uncertainty in $\tau_{elastic}$ for unloading steps, we focus primarily on stable unloading steps and we do not use data from unstable unloading steps in our analysis below.

3.1. Parameter α

[17] *Linker and Dieterich* [1992] defined a parameter α to study the evolution in shear strength upon a step change in normal stress. The parameter α is the normalized frictional response to a normal stress step, defined as

$$\alpha = \frac{\Delta\tau_\alpha/\sigma}{\ln(\sigma/\sigma_0)}; \quad (1)$$

α lies between 0 and the friction coefficient at steady state μ_{ss} [*Perfettini et al.*, 2001]. When $\alpha = \mu_{ss}$, there is no instantaneous change in shear stress upon the step change in normal stress and $\Delta\tau_e = 0$. A similar parameter arises in the treatment of *Sleep* [1997].

[18] To provide a robust estimate of alpha based on many data, we fit a least squares best fit line, constrained to pass through the origin, to measurements of $\Delta\tau_\alpha/\sigma$ plotted against $\ln(\sigma/\sigma_0)$ (Figure 5). We used data from step tests conducted for shear displacements of 15–20 mm, following the loading procedure detailed in Figure 1. For quartz gouge sheared at V = 30 μm/s and subject to step increases in normal stress, we obtained $\alpha = 0.331$ (Figure 5a). Data from two independent and identical experiments, p276 and p280, show excellent reproducibility and indicate that α is well constrained (Figure 5a). The parameter α is also well constrained for quartz-clay gouge (Figure 5b). We find a linear relationship between the transient change in friction $\Delta\tau_\alpha/\sigma$ and the magnitude of the normal stress change $\ln(\sigma/\sigma_0)$. However, data for stress increases differ from those for stable normal stress decreases; $\alpha = 0.230$ and 0.120, respectively (Figure 5b). Similar results are found using measurements of $\Delta\tau_\alpha$ for unstable unloading steps (e.g., Figure 4c).

3.2. Effect of Sliding Velocity

[19] We studied the relationship between loading velocity and parameter α following the loading

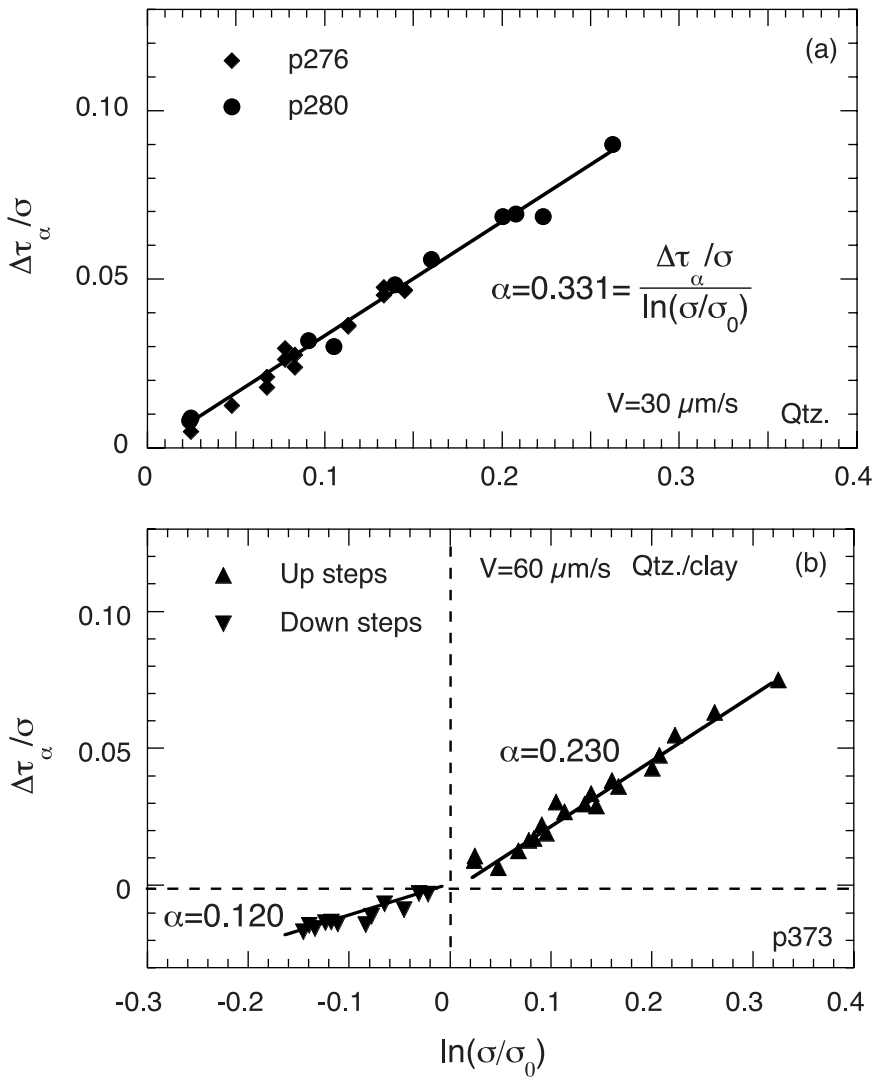

Figure 5. The nonelastic part of the change in frictional strength due to a normal stress perturbation is plotted versus the magnitude of the normal stress step. The parameter α is the slope of the best fit line through the origin. (a) Data from layers of quartz gouge subject to positive stress steps, showing $\alpha = 0.331$. (b) Data from layers composed of a clay-quartz mixture subject to positive and negative stressing. The parameter α is lower than that for pure quartz and differs for loading and unloading.

procedure described above and by systematically varying loading velocity during normal step tests (e.g., Figure 1) from 3 to 1000 μm/s. Two sets of normal stress steps were conducted and values of α were obtained from the displacement range 15–20 mm, as above (Figure 1). Three normal stress histories were used to obtain a range of stress perturbation magnitudes. History1: 20 to 20.5 to 21.5 to 23 to 25 to 28 to 32 to 37 to 40 to 37 to 32 to 28 to 25 to 23 to 20 MPa. History2: 10 to 11 to 13 to 16 to 20 to 20.5 to 21 to 23 to 22.5 to 21.5 to 19 to 17 to 14 to 12 to 10 MPa. History3: 10 to 13 to 18 to 20 to 23 to 27 to 33 to 32 to 30 to 27 to 24 to 20 to 17 to 12 to 10 MPa.

[20] Parameter α did not change systematically with sliding velocity for either quartz or clay-rich gouge (Figure 6). However, α was significantly larger for quartz gouge compared to clay-quartz gouge. For quartz gouge (Figure 6a), α ranged from 0.28–0.37, and small normal stress reductions tended to induce dynamic instability (e.g., Figure 2a). In contrast, for clay-rich gouge, α ranged from 0.07 to 0.24 and was systematically larger for loading (0.15–0.24) steps compared to unloading steps (0.07–0.12) (Figure 6b). The clay-rich gouge exhibited stable sliding during even large step reductions of normal stress (e.g., Figure 2b).

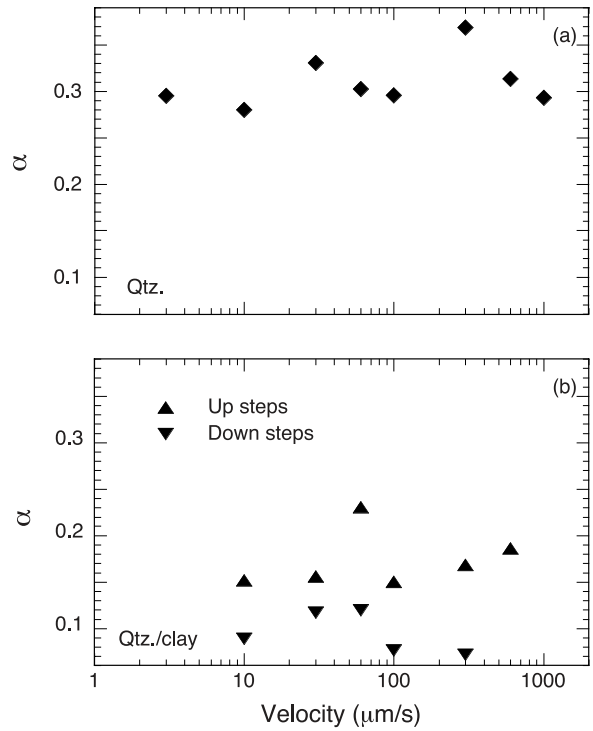

Figure 6. Measurements of parameter α as a function of loading velocity from (a) stress increases on layers of pure quartz and (b) both increases and decreases of stress on layers of clay-quartz. The parameter α does not vary systematically with velocity over this range. For layers composed of the clay-quartz mixture, α is larger for stress increases than for unloading steps.

3.3. Effect of Displacement

[21] As slip and shear strain accumulates, pervasive shearing within gouge changes to localized shearing along oblique and boundary parallel shear bands. Also, previous work shows that gouge changes from a velocity strengthening frictional regime associated with pervasive strain to a velocity weakening regime associated with the development of boundary parallel shears. To evaluate the effect of net shear strain on α, we ran a suite of experiments in which normal stress-stepping tests were conducted throughout shear (Figure 7). Instead of load cycles and velocity stepping before normal stress step tests, we used a constant loading rate of 30 μm/s and imposed identical sets of normal stress steps at established displacements. Normal stress step tests began after steady state shear strength was reached and before the transition from velocity strengthening to velocity weakening frictional behavior (Figure 7). Six sets of normal stress step tests were conducted and, even at the scale of Figure 7a, it is clear that the magnitude of the frictional response, and the degree of instability for unloading steps varies with accumulated displacement.

[22] The shear stress responses to identical unloading steps (from 23 to 22 MPa) for three successive sections are highlighted in Figure 7c. These data indicate a clear transition from stable to nearly unstable and then to fully unstable behavior (Figure 7c). This behavior was robust and reproducible in all tests with quartz gouge.

[23] We measured α from each set of normal stress increases as a function of increasing displacement (Figure 8). For quartz gouge, α decreased appreciably with displacement, ranging from 0.282 for the steps that began at 7.5 mm to 0.215 for steps that began at 27 mm. α also decreased for clay-quartz gouge, ranging from 0.192 to 0.160 (Figure 8). For shear between Westerly granite blocks without gouge, α was approximately independent of displacement (Figure 8c). Comparison of the data from Figure 6 at V = 30 μm/s with that of Figure 8 shows that α depends on loading history in addition to net displacement; α values for gouge subject to shear load cycling at high normal stress (e.g., Figure 1) are higher than those obtained using the procedure of Figure 7.

3.4. Effect of Humidity

[24] We explored the effect of humidity on the frictional response to normal stress perturbations by conducting experiments following the procedure of Figure 1 at high (40–50%) and low (10–15%) relative humidity at room temperature. Figure 9 shows the measurements of α for pure quartz and clay-quartz gouge at different levels of relative humidity. As humidity increased from 11% to 51% for pure quartz, α increased from 0.264 to 0.331. The transient response of frictional strength to a normal stress perturbation is larger for higher humidity (e.g., Figure 3). In contrast, as humidity increased from 13% to 40% for the clay-quartz gouge, α decreased from 0.177 to 0.156, indicating a smaller value of $\Delta\tau_\alpha$ at higher humidity. Repeat experiments at a given humidity (Figure 9b) show excellent reproducibility. Our data show that humidity influences the frictional response to normal stress and that the effect for pure quartz gouge and clay-quartz mixtures are opposite.

3.5. Critical Distance for Transient Friction Evolution

[25] Upon a step increase in normal stress, shear stress increases immediately along the elastic linear

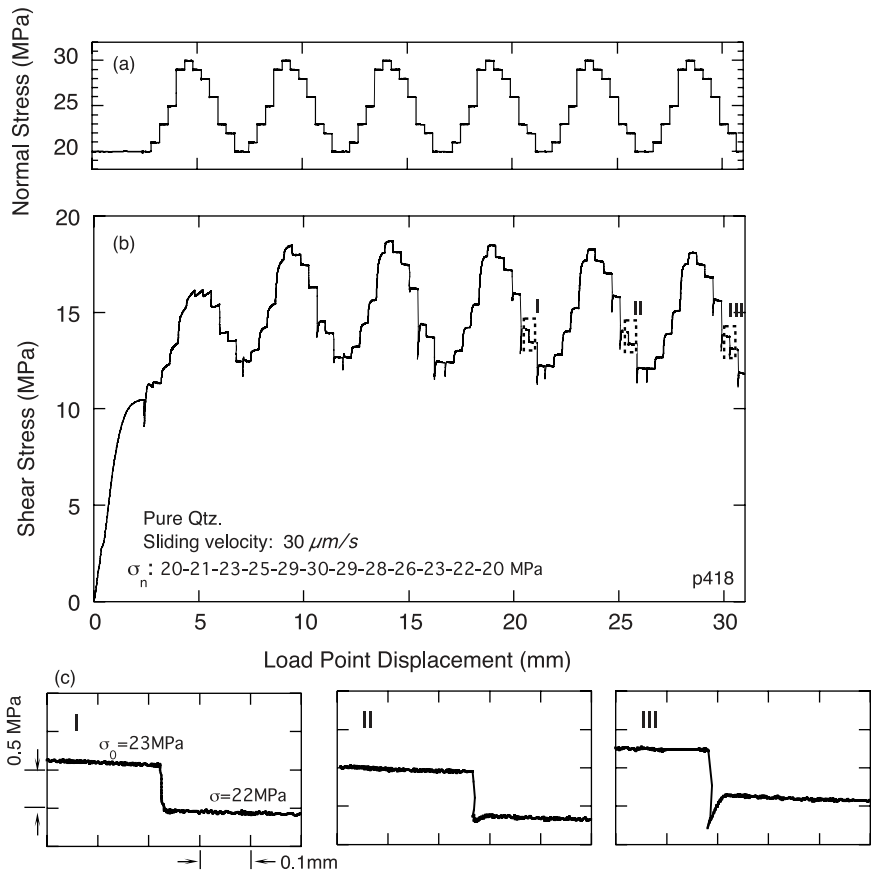

Figure 7. (a) Imposed normal stress history and (b) shear response for an entire experiment showing evolution in strength behavior as a function of shear displacement. Six identical segments of normal stressing are shown. Dashed boxes in Figure 7b are enlarged in Figure 7c, which shows that as slip evolves the response to normal stress unloading changes from stable (I) to nearly unstable (II) and fully unstable (III).

loading curve until $\tau_{elastic}$ and then strength increases gradually to a new steady state over distance d_α (Figure 3). We measured d_α for gouge sheared at a range of sliding velocities and stress perturbation magnitudes (Figure 10). With increasing magnitude of the normal stress perturbation, d_α increased and became constant for the largest stress steps, independent of sliding velocity. For quartz/clay gouge, d_α saturated at about 275 μm for stress jumps above ~6% of the nominal normal stress (Figure 10). For quartz gouge d_α increases to 200–250 μm for the largest stress jumps. Values for granite are significantly smaller, ranging from 10 μm for a 2% change in normal stress to 30–40 μm for a 10–12% change in normal stress. These results are consistent with the ideas of *Sleep et al.* [2000].

[26] One of our goals was to investigate whether the transient friction evolution is best described by a characteristic slip or time. The data of Figure 10 show that evolution occurs over a characteristic displacement rather than a characteristic time. If the evolution were time-dependent, rather than displacement-dependent, d_α would vary by approximately a factor of 30 for V = 30 and 1000 μm/s, which is clearly not observed (Figure 10).

4. Discussion

[27] Our data show that normal stress perturbations during steady creep have a complex effect on the frictional strength of both bare rock surfaces and layers of simulated fault gouge. Step changes in normal stress result in an immediate, elastic change in shear stress followed by an evolution of frictional strength over a characteristic displacement. Given the utility of rate and state dependent friction laws for modeling earthquake phenomena, one important question is that of whether our data can be fit with this type of law.

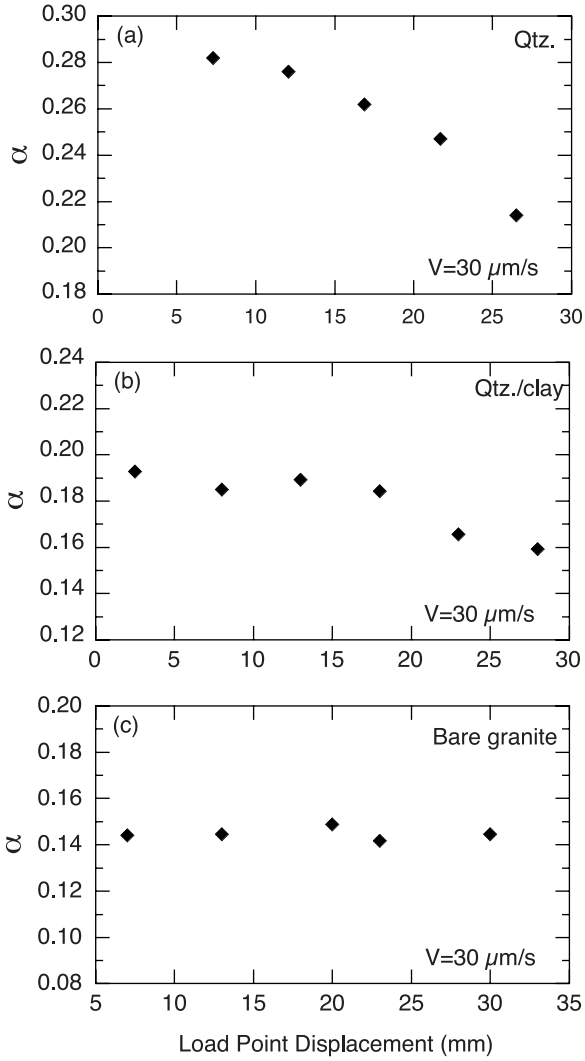

Figure 8. Friction parameter α as a function of load point displacement for (a) pure quartz, (b) clay-quartz mixture, and (c) bare surfaces of Westerly granite. Parameter α is independent of displacement for bare Westerly; however, α decreases with net displacement for gouge layers, and the reduction is more pronounced for layers of pure quartz.

[28] The rate- and state-dependent constitutive relationship for shear stress τ is as follows [*Dieterich*, 1979; *Ruina*, 1983]:

$$\tau = \sigma \cdot \left[\mu_0 + a \ln\left(\frac{V}{V_0}\right) + b \ln\left(\frac{V_0\theta}{D_c}\right)\right], \qquad (2)$$

where μ_0 represents a constant reference value of friction at steady state sliding velocity V_0; the scalar variable θ represents the state of the sliding surface, which can be interpreted as mean porosity for gouge or the average lifetime of surface contacts; D_c is the characteristic evolution displacement needed to go from one steady state to a new steady state; and a and b are dimensionless empirical parameters that are estimated from laboratory tests.

[29] The two most common evolution laws, the Dieterich law and the Ruina law, were tested in our modeling. These two rate/state friction laws were extended by *Linker and Dieterich* [1992] and *Perfettini et al.* [2001] to account for variable normal stress as

$$\text{Dieterich} \qquad \frac{d\theta}{dt} = 1 - \frac{V\theta}{D_c} - \alpha\frac{\theta}{b\sigma}\frac{d\sigma}{dt}, \qquad (3)$$

$$\text{Ruina} \qquad \frac{d\theta}{dt} = -\frac{V\theta}{D_c}\ln\left(\frac{V\theta}{D_c}\right) - \alpha\frac{\theta}{b\sigma}\frac{d\sigma}{dt}. \qquad (4)$$

[30] The term α, defined in equation (1), describes the evolution of shear stress associated with variable normal stress. Increased α results in an increased evolutional response of shear stress for a perturbation in normal stress (Figure 3).

[31] Elastic distortion and interaction between the slipping surfaces and our testing apparatus was modeled with a single degree of freedom relationship as

$$\frac{d\tau}{dt} = K \cdot (V_{lp} - V), \qquad (5)$$

where K is the apparatus stiffness and V_{lp} is the load point velocity, which was set equal to V_0 in (2) for modeling.

[32] The immediate change in state variable θ caused by a step change in normal stress from σ_0 to σ is given by

$$\theta = \theta_0\left(\frac{\sigma_0}{\sigma}\right)^{\alpha/b}. \qquad (6)$$

[33] Typically, α is much larger than b, so the state variable immediately decreases upon a step increase in normal stress. This can be thought of as a decrease of the average porosity of fault gouge or a decrease in the average lifetime of asperity contacts, since new contacts are created by the sudden compression associated with increased normal stress. Conversely, the state variable immediately increases upon a step decrease in normal stress, since the ratio σ_0 to σ (which is <1) is raised to a power >1. Physically, this decrease in frictional state can be thought of as an increase in gouge porosity caused by the reduction in normal stress. In terms of contact mechanics, the decrease in θ implies a decrease in average contact junction

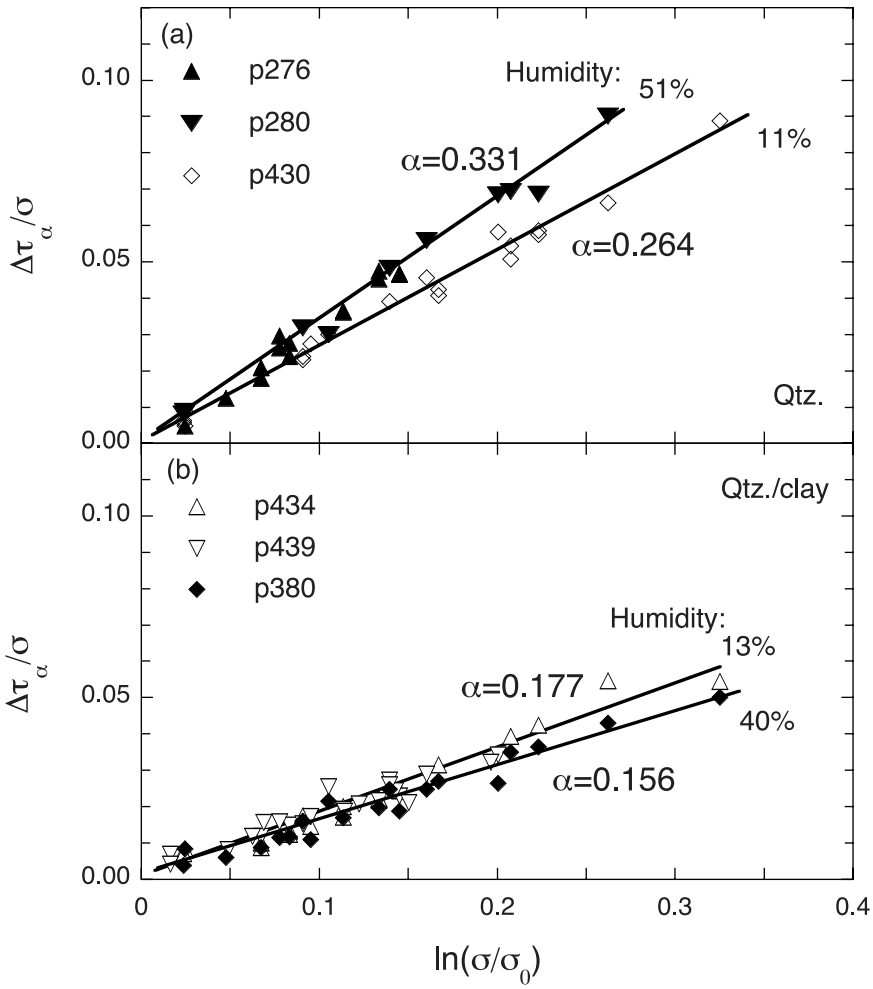

Figure 9. The parameter α as determined for different ambient humidity conditions for (a) pure quartz gouge and (b) gouge layers composed of quartz-clay mixtures. For quartz, α is larger for higher humidity: α is 0.331 for 51% relative humidity (p276, p280) and 0.264 for 11% relative humidity (p 430). For the clay-quartz gouge, α is lower for higher humidity: α = 0.177 for 13% RH (p434, p439) and α = 0.156 for 40% RH (p380).

age, which is consistent with preferential loss of the youngest and weakest contacts, including those with the least interpenetration and local plastic deformation [e.g., *Dieterich and Kilgore*, 1994]. After the immediate change in state, θ evolves according to the standard rate-state law via either (3) or (4) with dσ/dt = 0.

[34] We modeled our data using both the Dieterich and the Ruina laws by solving (2), (5), (6) with either (3) or (4) simultaneously using a fifth-order Runga-Kutta method [*Press et al.*, 1992]. The parameter α was measured as described above and we used the values given in Figure 6 for the modeling results presented in Figure 11. Parameters a, b, and D_c were obtained by a least squares iterative inversion of data from velocity stepping carried out during the same experiment before normal stress stepping. The following values were obtained from our experiments: $a = 0.0073$, $b = 0.0076$, $D_c = 40$ μm for pure quartz gouge (Figures 11a and 11b) and $a = 0.0058$, $b = 0.0045$, $D_c = 75$ μm for clay-quartz mixtures (Figures 11c and 11d).

[35] We compare predictions of rate-state friction with our data for step increases in normal stress on pure quartz and clay-quartz mixtures (Figure 11). Because the rate-state parameters have been determined independently, there are no free parameters in the fits shown in Figure 11. In all cases, the Ruina law matches the laboratory data significantly better than does the Dieterich law. The Dieterich law predicts a sharper approach to steady state than the data. In addition, the Dieterich law sometimes overshot the final steady state shear stress (Figure 11a), which was not observed in the

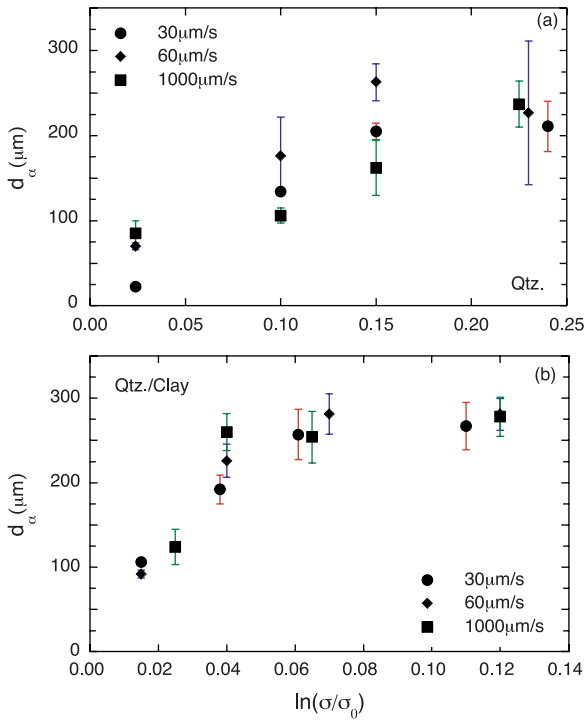

Figure 10. The evolution distance d_α versus $\ln(\sigma/\sigma_0)$ of three different sliding velocities for (a) pure quartz and (b) clay-quartz gouge. The error bars represent ±1 standard deviation. The parameter d_α increases with increasing stress step magnitude, and there is some indication of a saturation of d_α for the largest stress jumps. Within the scatter, d_α does not vary with velocity. These data show that frictional strength evolves over a characteristic displacement, d_α, rather than a characteristic time interval.

laboratory data. Our data show that the shear stress response to a step increase in normal stress is consistent with the rate- and state-dependent constitutive laws. We note that the rate- and state-dependent relationships do not incorporate displacement and humidity effects, and thus we interpret these results primarily in terms of particle characteristics and contact mechanics.

4.1. Micromechanical Model for Transient Friction Response

[36] According to *Wang and Scholz* [1994], individual contact junctions between gouge particles can be classified geometrically into those that involve primarily normal and oblique contact (Figure 12). For normal contacts, the normal stress distribution has a maximum value at the center while the shear stress distribution has a maximum value at the edges and a minimum at the center. Consequently, if the shear load increases, slipping will start at the edges, and propagate inward. Oblique contact is characterized by the contact angle (Figure 12b).

[37] As slip evolves, oblique contacts within gouge will be formed due to the initial overlap of the topography of gouge grains, which is often referred to as interlocking. This will increase friction accordingly and those oblique contacts with higher contact angle will have higher friction.

[38] Our data support the following interpretation based in part on the model of *Wang and Scholz* [1994]. Upon a step increase in normal stress, normal contact areas and contact angles will increase instantaneously. The increased pressure will promote fracture and hence result in formation of new grain contact areas. In addition, some highly stressed, fully sliding contacts will cease slipping and become partial sliding contacts, due to increased pressure (Figure 12a). With continued shear loading, shear stress will increase and new contacts will begin to slip. For partial sliding contacts, the annulus of slipping regions will propagate inward until c = 0 and they become fully sliding (Figure 12). These processes will result in a transient, nonlinear shear-displacement curve, such as observed in our experiments (e.g., Figure 3).

[39] Figure 13 schematically shows the responses of the real contact area of particle junctions (A_r) and shear stress versus load point displacement and interparticle slip following a step increase in normal stress. According to the above interpretation, under the suddenly increased normal stress, real contact area A_r increases instantaneously to a certain point $A_{relastic}$ followed by evolution with displacement along the nonlinear curve to a new steady state. As the real contact area of particle junctions determines the frictional properties, we posit that, upon a step increase in normal stress, this evolution in A_r produces the evolution in shear stress response ($\Delta\tau_\alpha$) characterized by parameter α. Therefore α is directly related to the gouge particle characteristics. For bare granite, it is closely related to the surface roughness and contact asperities. Due to elastic interaction between the load point and the shearing surface, shear stress increases linearly along the elastic loading path, followed by transient evolution of frictional strength (Figure 13a). When plotted versus mean interparticle slip, the increase in real contact area and shear stress is instantaneous (Figure 13b).

[40] The asymmetry in α observed for normal stress increases versus decreases (Figure 5) is also

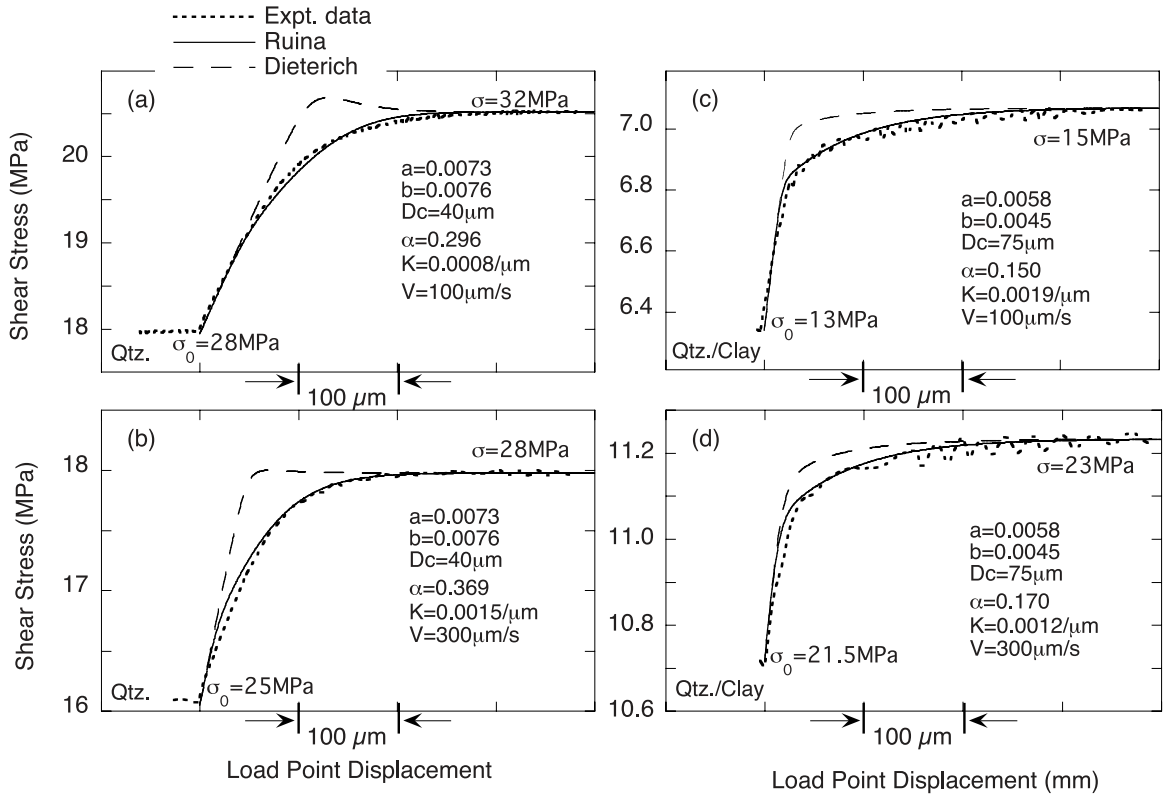

Figure 11. Experimental data and modeling results for a step increases in normal stress. (a and b) Quartz gouge. (c and d) Clay-quartz gouge. Two loading velocities are shown for each gouge. Frictional parameters a, b, D_c, and α were measured from velocity step tests and normal stress step tests in the same experiment. The Ruina law provides a better fit to the data than the Dieterich law.

consistent with an interpretation based on particle contact mechanics and fabric development. In clay-rich gouge, the inelastic change in friction characterized by α is likely due in part to nonreversible alignment of clay particles. Normal stress increases would enhance alignment locally within shear bands, which would result in larger α compared to normal stress reductions, for which clay particle alignment would be negligible.

4.2. Effect of Displacement

[41] Several previous works have documented a transition from velocity strengthening frictional behavior ($a - b > 0$) to velocity weakening behavior ($a - b < 0$) with increased shear displacement. *Marone et al.* [1992] and *Beeler et al.* [1996] correlated this transition with fabric development in gouge and showed that the transition from pervasive to localized shearing of fault gouge is associated with a transition from velocity strengthening to velocity weakening frictional behavior.

[42] Our data also show a clear transition in the shear response to a normal stress step as a function of accumulated shear strain. The shear responses to unloading at shear strains of 8, 10, and 12 show a transition from stable to nearly unstable and then to fully unstable shear behavior, respectively (Figure 7c). These observations are consistent with a transition from intrinsically stable behavior ($a - b > 0$) to potentially unstable behavior ($a - b < 0$). In addition to the change in ($a - b$), we document a systematic change in α with increasing shear strain (Figure 8). For the displacement interval 5–30 mm, α decreases more rapidly for quartz gouge than for quartz-clay gouge. Taken together with the generally lower values for quartz-clay gouge, the observations are consistent with a more rapid evolution to a steady state particle size distribution and gouge fabric for the mixed gouge. Whereas layers of pure quartz may undergo significant grain comminution during fabric development, we posit that clay grains shield quartz particles and decrease the tendency for fracture.

[43] In contrast to the results for gouge, α was approximately constant for bare granite surfaces through the same displacement range. Taken to-

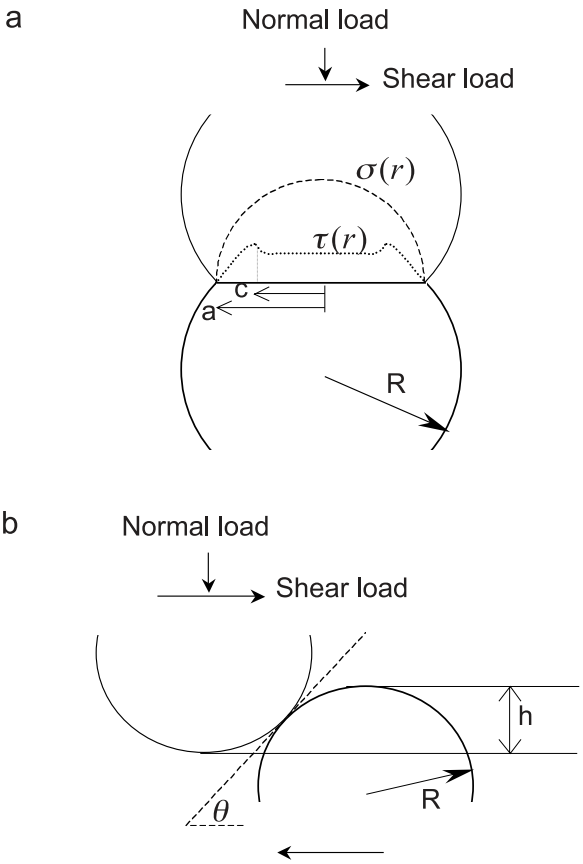

Figure 12. (a) Contact of two grains under normal and shear load. The contact area is circular with radius *a*. The normal stress distribution σ(r) is shown by the dashed line, and the shear stress distribution τ(r) is indicated by the dotted line. The annular boundary between the slipped and locked region is at *c*. (b) Oblique contact of two grains with overlap distance h and contact angle θ.

gether with the larger values of α for gouge, this is consistent with the above particle-based interpretation of α. That is, the transient part of the shear strength response to a stress step is larger for gouge than for bare rock surfaces because shear occurs within a finite volume containing many particle contacts, and each particle-particle contact junction has its own nonlinear response. Some of these many-particle interactions will proceed serially, as slip along one interparticle contact causes loading of neighboring contacts, which then slip and respond nonlinearly. Following the model of *Marone and Kilgore* [1993] for the critical friction distance, we posit that the transient shear response of a gouge layer to a normal stress step is an ensemble average over many particle contacts and that α and d_α scale with gouge layer thickness or shear band thickness. Our data for d_α support this hypothesis (Figure 10), showing that d_α is significantly smaller for bare surfaces compared to shear within a finite thickness of a gouge layer.

[44] To investigate the role of shear strain and fabric development, we introduce two new terms, $\alpha_{elastic}$ and α_{total} (e.g., Figure 3), which are defined by the elastic $\Delta\tau_e$ and total $\Delta\tau_t$ change in shear strength, respectively, for a normal stress perturbation:

$$\alpha_{elastic} = \frac{\Delta\tau_e/\sigma}{\ln(\sigma/\sigma_0)}, \tag{7}$$

$$\alpha_{total} = \frac{\Delta\tau_t/\sigma}{\ln(\sigma/\sigma_0)}. \tag{8}$$

We measured $\alpha_{elastic}$ and α_{total} using the same approach used for α, by fitting a line through the

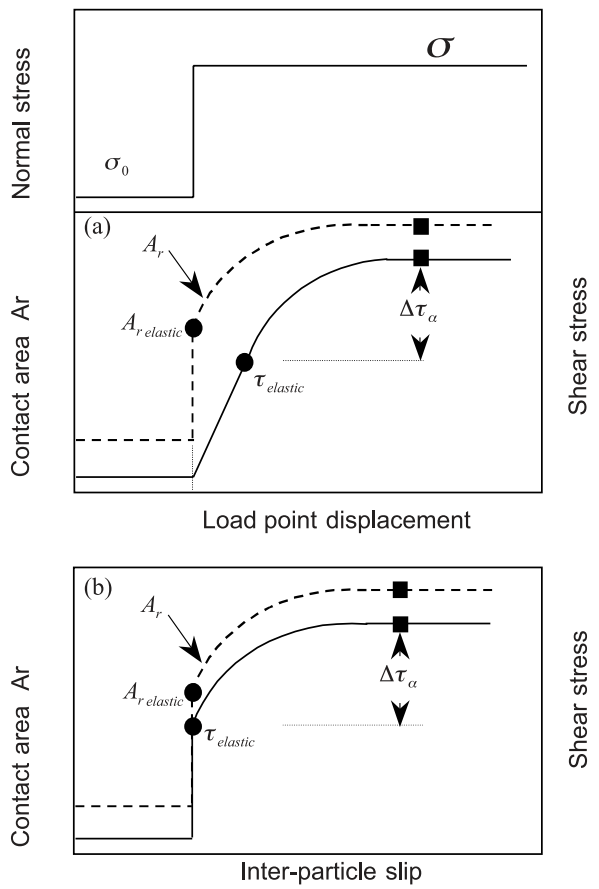

Figure 13. Schematic illustration of the response of asperity contact area and shear stress versus (a) load point displacement and (b) interparticle slip following a step increase in normal stress. The evolution in real contact area causes the evolution in shear strength ($\Delta\tau_\alpha$) that determines parameter α.

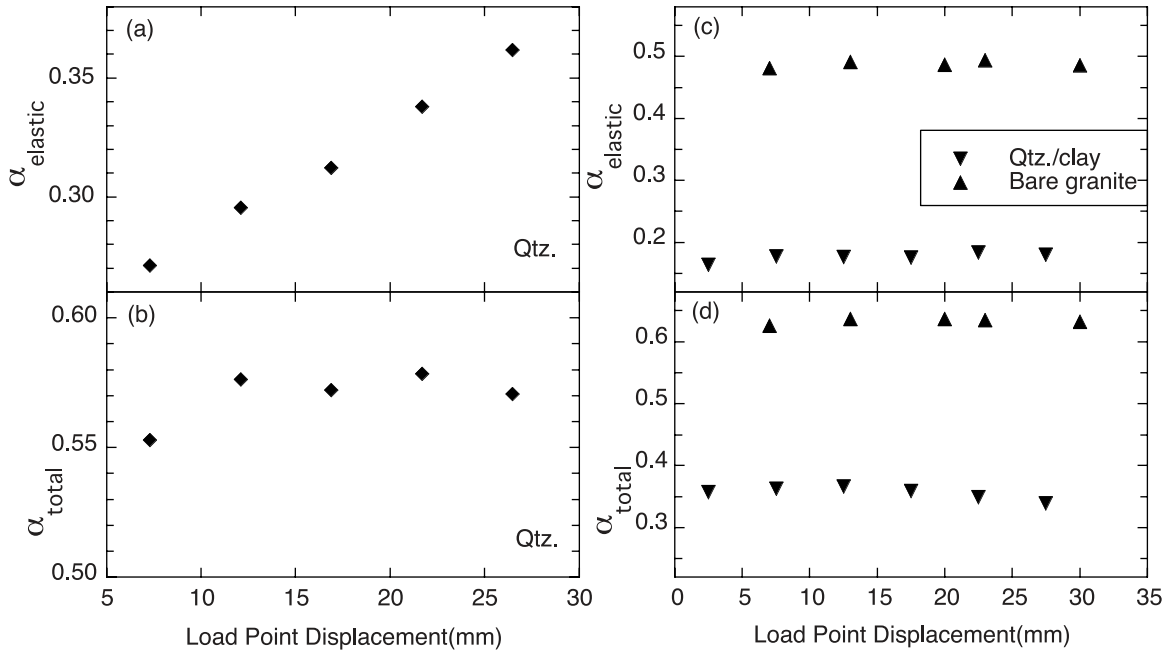

Figure 14. The elastic and inelastic parts of frictional strengthening (see Figure 3). (a) $\alpha_{elastic}$ and (b) α_{total} versus load point displacement for three different materials. For pure quartz, $\alpha_{elastic}$ increased linearly with slip, while α_{total} was nearly constant. This shows that the decrease in α with slip (Figure 8) is due to increased elastic strengthening. For clay-quartz gouge and bare granite surfaces, both $\alpha_{elastic}$ and α_{total} were constant with displacement.

origin to measurements of $\Delta\tau_e/\sigma$ and $\Delta\tau_t/\sigma$ plotted against $\ln(\sigma/\sigma_0)$, respectively. For quartz gouge $\alpha_{elastic}$ increases linearly with displacement while α_{total} becomes constant for displacements greater than 15 mm (Figure 14). The elastic part of the frictional response to normal loading ranges from 50 to 64%. Comparison with the results for α (Figure 8) shows that the strong displacement-dependent decrease in α is compensated by an increase in $\alpha_{elastic}$. The progressive changes in $\alpha_{elastic}$ and α are consistent with the effects of grain size reduction and fabric development, which continue for this displacement range and normal stress [*Beeler et al.*, 1996; *Mair and Marone*, 1999]. For granite surfaces and quartz-clay gouge, both $\alpha_{elastic}$ and α_{total} are independent of displacement (Figure 14). Although granite surfaces exhibit the smallest transient change in frictional strength (Figure 8) they have the largest elastic and total change in strength (Figure 14).

[45] For the quartz-clay gouge, the combination of a large particle size distribution and the presence of small, plate-like clay grains would allow a compact gouge fabric to be created during initial loading before our normal stress stepping procedure. This early formed compact fabric implies that comminution is negligible during the normal stress stepping procedure. These factors would tend to limit the increase in contact area for an increase in normal stress, which explains why $\alpha_{elastic}$ remains approximately constant with increased displacement (Figure 14c). Sheet-structure minerals within gouge typically rotate until their planes are parallel to the shearing direction, which would reduce the gouge strength. This is consistent with our observations of α_{total} on the mixtures with the presence of sheet-structure clay (Figure 14d). That is, α_{total} was lowest and decreased slightly with increased displacement. This implies that the slow decrease in α (Figure 8b) is a consequence of the slow decrease in α_{total}.

4.3. Effect of Humidity

[46] Water content has been correlated with important changes in frictional properties [*Dieterich and Conrad*, 1984; *Frye and Marone*, 2002; *Moore and Lockner*, 2004]. The ability of gouge materials to absorb water onto the particle surfaces or to accommodate interlayer water within crystal structures has a strong influence on the frictional strength. *Frye and Marone* [2002] found that water content did not affect the residual frictional strength of quartz gouge. However, *Morrow et al.* [2000] and *Moore and Lockner* [2004] showed that

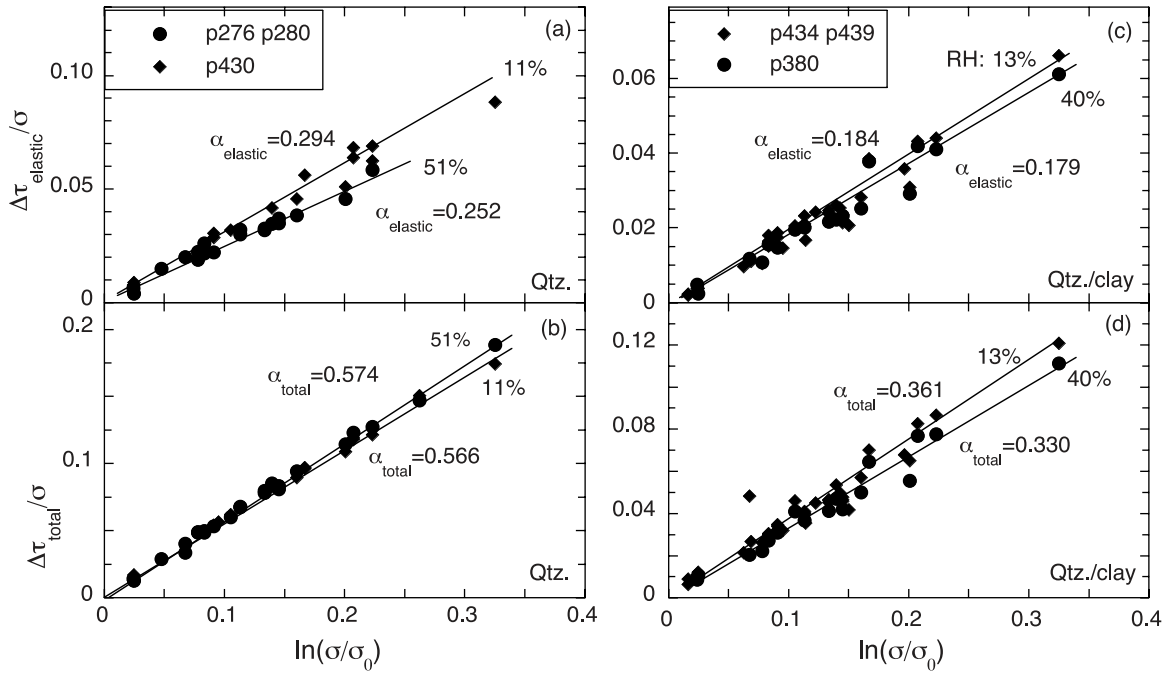

Figure 15. Humidity dependence of the elastic and inelastic parts of frictional strengthening (see Figure 3) for quartz and clay-quartz gouge. For quartz gouge, $\alpha_{elastic}$ decreased with increasing humidity and α_{total} was independent of humidity. For clay-quartz gouge, $\alpha_{elastic}$ was independent of humidity and α_{total} decreased as humidity increased.

the frictional strength of smectite clay was reduced up to 60% with water saturation. These studies suggest that for sheet-structure mineral powders (like the smectite clay in our study), the bound, interlayer water influences frictional strength significantly.

[47] Our data show that increased humidity resulted in increased α for pure quartz gouge while causing decreased α for quartz-clay mixtures (Figure 9). We also measured $\alpha_{elastic}$ and α_{total} as a function of humidity (Figure 15). For quartz gouge, $\alpha_{elastic}$ was higher at higher humidity but α_{total} was independent of humidity. In contrast, for clay-quartz gouge, humidity had no obvious effect on $\alpha_{elastic}$, while it had a clear effect on α_{total} (Figure 15). *Frye and Marone* [2002] found that water content did not affect the mean coefficient of sliding friction μ_{ss} for quartz gouge, which is consistent with our data showing that α_{total} was independent of humidity (Figure 15b). One possible explanation is that quartz particle surfaces are for the most part electrically neutral compared to clay particles, so the attracted water layers are only loosely bonded, therefore unable to provide a low-resistance slip interface [*Moore and Lockner*, 2004].

[48] Adsorbed water layers might have an effect on the response to changes in normal stress. For example, in the relatively humid case, more adsorbed water on grain surfaces might mean that it is easier to squeeze out the water to allow stronger quartz-quartz bonding, effecting a larger change in shear stress with a change in normal stress than in the dry case, as is observed for quartz gouge. If the thickness of the water layer within contacts decreases at lower humidity, it would be more difficult to squeeze out the water, such that changes in normal stress would have a lesser effect on across-contact bonding (and hence shear strength) than in the wet case. This interpretation is consistent with our data for quartz, which shows an increase in α and reduction in $\alpha_{elastic}$ at higher humidity (Figures 9 and 15). In contrast, higher humidity decreases α for clay rich gouge. If part of the origin of α involves time- or shear-induced removal or adsorbed species from highly stressed contacts, then the observation of lower α clay-rich gouge, compared to pure quartz, is consistent with adsorbed species being more strongly bound to clay surfaces. The reduction of α at higher humidity in clay-rich gouge is consistent with previous work showing that clay friction decreases dramatically in the presence of bound water.

[49] Water is known to enhance both point defect and dislocation migration in single-crystal quartz, quartz-aggregate and quartzite systems [*Blacic and Christie*, 1984; *Jaoul et al.*, 1984; *Mainprice and Paterson*, 1984; *Kronenberg and Tullis*, 1984]. This water-assisted plastic deformation, known as hydrolytic weakening, could be a mechanism by which the contact area grows with time. *Frye and Marone* [2002] showed that hydrolytic weakening influences the friction evolution effect and time-dependent frictional healing for quartz and alumina. Absorbed water on the surfaces of quartz particles could enable hydrolytic weakening and hence time-dependent contact area growth [*Hirth and Rice*, 1980; *Dieterich and Conrad*, 1984; *Michalske and Fuller*, 1985]. If hydrolytic weakening were inhibited in the relatively low humidity cases we studied, time-dependent contact area growth would be smaller for a given (sudden) increase in pressure. Therefore α would be smaller for the lower humidity case, which is consistent with our results (Figure 9). Moreover, in the absence of hydrolytic weakening, contact stresses would be higher and elastic effects more pronounced, which would explain our observation of higher $\alpha_{elastic}$ for the low humidity case (Figure 15a).

5. Conclusions

[50] We studied normal stress perturbations during steady frictional shear of pure quartz gouge, bare surfaces of Westerly granite, and a gouge composed of a mixture of quartz and clay. For each case, we find that a sudden increase in normal stress causes shear stress to increase immediately along the elastic loading curve followed by a gradual evolution of shear strength over a characteristic displacement d_α. Upon a step decrease in normal stress, either the opposite occurred or instability was induced. We found that the magnitude of the transient change in frictional strength, α, (1) was independent of sliding velocity over the range 3 μm/s to 1 mm/s for all materials, (2) was larger for step increases of normal stress compared to step decreases, (3) decreased with shear displacement for gouge but not bare granite surfaces, and (4) increased with increasing humidity in quartz gouge but decreased for clay-rich gouge. Our data show that α differs for bare rock surfaces versus shear within granular and clay rich gouge. Parameter α was larger for quartz gouge compared to clay-quartz mixtures for a given set of conditions. Rate and state friction laws match our results for normal stress step experiments, with the Ruina evolution law providing a significantly better fit to our data than the Dieterich law.

[51] We document a transition from stable to unstable behavior for unloading perturbations of normal stress as a function of increasing shear strain. This phenomenon was observed for the first time in our experiments and is related to the transition in friction velocity dependence with displacement due to the transition from pervasive to localized shear. The displacement effect on α was interpreted in terms of particle size distribution and gouge fabric development.

[52] Our data show that humidity has important effects on the frictional properties of gouge. Increased water content decreased the strength of clay-quartz gouge but did not affect the strength of pure quartz gouge, in accord with previous studies. Humidity effects on α were interpreted in terms of a model based on contact mechanics and particle size distribution. The experiments show that fault zone friction exhibits significant departure from simple models based on Coulomb friction and that these transient, inelastic behaviors are important for understanding fault interaction and earthquake triggering.

Acknowledgments

[53] We would like to thank M. Boettcher and J. Anthony for technical expertise and helpful discussions and J. Rice and J. Dieterich for helpful discussions. This paper benefited from the insightful reviews of G. Beroza and two anonymous reviewers. This research was supported by NSF grant EAR 03-37627, USGS grant 02HQGR0156, and NSF grant OCE-0196462.

References

Beeler, N., T. Tullis, M. Blanpied, and J. Weeks (1996), Frictional behavior of large displacement experimental faults, *J. Geophys. Res.*, *101*(B4), 8697–8715.

Ben-Zion, Y. (2001), Dynamic ruptures in recent models of earthquake faults, *J. Mech. Phys. Solids*, *49*, 2209–2244.

Blacic, J. D., and J. M. Christie (1984), Plasticity and hydrolytic weakening of quartz single crystals, *J. Geophys. Res.*, *89*, 4223–4240.

Boettcher, M. S., and C. Marone (2004), Effects of normal stress variation on the strength and stability of creeping faults, *J. Geophys. Res.*, *109*, B03406, doi:10.1029/2003JB002824.

Bouchon, M., and D. Streiff (1997), Propagation of a shear crack on a non-planar fault: A method of calculation, *Bull. Seismol. Soc. Am.*, *87*, 61–66.

Bureau, L., T. Baumberger, and C. Caroli (2000), Shear response of a frictional interface to a normal load modulation, *Phys. Rev. E*, *62*, 6810–6820.

Cochard, A., and J. R. Rice (2000), Fault rupture between dissimilar materials: Ill-posedness, regularization, and slip-pulse response, *J. Geophys. Res.*, *105*(B11), 25,891–25,907.

Cochard, A., L. Bureau, and T. Baumberger (2003), Stabilization of frictional sliding by normal load vibrations, *J. Appl. Mech.*, *70*, 220–226.

Dieterich, J. H. (1979), Modeling of rock friction: 1. Experimental results and constitutive equations, *J. Geophys. Res.*, *84*, 2161–2168.

Dieterich, J. H., and G. Conrad (1984), Effect of humidity on time and velocity-dependent friction in rocks, *J. Geophys. Res.*, *89*, 4196–4202.

Dieterich, J. H., and B. Kilgore (1994), Direct observation of frictional contacts: New insights for state-dependent properties, *Pure Appl. Geophys.*, *143*, 283–302.

Frye, K. M., and C. Marone (2002), Effect of humidity on granular friction at room temperature, *J. Geophys. Res.*, *107*(B11), 2309, doi:10.1029/2001JB000654.

Gomberg, J. (1996), Stress/strain changes and triggered seismicity following the M_w 7.3 Landers, California, earthquake, *J. Geophys. Res.*, *101*(B1), 751–764.

Gomberg, J., and P. Bodin (1994), Triggering of the *Ms* = 5.4 Little Skull Mountain, Nevada, earthquake with dynamic strains, *Bull. Seismol. Soc. Am.*, *84*(3), 844–853.

Gomberg, J., and S. Davis (1996), Stress/strain changes and triggered seismicity at the Geysers, California, *J. Geophys. Res.*, *101*(B1), 733–750.

Gomberg, J., M. L. Blanpied, and N. M. Beeler (1997), Transient triggering of near and distant earthquakes, *Bull. Seismol. Soc. Am.*, *87*(2), 294–309.

Harris, R. A. (1998), Introduction to special section: Stress triggers, stress shadows, and implications for seismic hazard, *J. Geophys. Res.*, *103*(B10), 24,347–24,358.

Harris, R. A., and S. M. Day (1993), Dynamics of fault interaction: Parallel strike-slip faults, *J. Geophys. Res.*, *98*, 4461–4472.

Hill, D., et al. (1993), Seismicity remotely triggered by the magnitude 7.3 Landers, California, earthquake, *Science*, *260*, 1617–1623.

Hirth, J. P., and J. R. Rice (1980), On the thermodynamics of adsorption at interfaces as it influences decohesion, *Metall. Trans. A*, *11*, 1501–1511.

Jaoul, O., J. Tullis, and A. K. Kronenberg (1984), The effect of varying water contents on creep behavior of Heavitree quartzite, *J. Geophys. Res.*, *89*, 4298–4312.

Kilb, D., J. Gomberg, and P. Bodin (2000), Aftershock triggering by complete Coulomb stress changes, *Nature*, *408*, 570–574.

Kilb, D., J. Gomberg, and P. Bodin (2002), Aftershock triggering by complete Coulomb stress changes, *J. Geophys. Res.*, *107*(B4), 2060, doi:10.1029/2001JB000202.

Kronenberg, A. K., and J. Tullis (1984), Flow strengths of quartz aggregates: Grain size and pressure effects due to hydrolytic weakening, *J. Geophys. Res.*, *89*, 4281–4297.

Linker, M. F., and J. H. Dieterich (1992), Effects of variable normal stress on rock friction: Observations and constitutive equations, *J. Geophys. Res.*, *97*, 4923–4940.

Mainprice, D. H., and M. S. Paterson (1984), Experimental studies of the role of water in the plasticity of quartzites, *J. Geophys. Res.*, *89*, 4257–4270.

Mair, K., and C. Marone (1999), Friction of simulated fault gouge for a wide range of velocities and normal stress, *J. Geophys. Res.*, *104*(B12), 28,899–28,914.

Marone, C., and B. Kilgore (1993), Scaling of the critical slip distance for seismic faulting with shear strain in fault zones, *Nature*, *362*, 618–621.

Marone, C., B. E. Hobbs, and A. Ord (1992), Coulomb constitutive laws for friction: Contrasts in frictional behavior for distributed and localized shear, *Pure Appl. Geophys.*, *139*, 195–214.

Michalske, T. A., and E. R. Fuller Jr. (1985), Closure and repropagation of healed cracks in silicate glass, *J. Am. Ceram. Soc.*, *68*, 5586–5590.

Moore, D. E., and D. A. Lockner (2004), Crystallographic controls on the frictional behavior of dry and water-saturated sheet structure minerals, *J. Geophys. Res.*, *109*, B03401, doi:10.1029/2003JB002582.

Morrow, C. A., D. E. Moore, and D. A. Lockner (2000), The effect of mineral bond strength and absorbed water on fault gouge frictional strength, *Geophys. Res. Lett.*, *26*(6), 815–818.

Oglesby, D. D., R. J. Archuleta, and S. B. Niielsen (1998), Earthquakes on dipping faults: The effects of broken symmetry, *Science*, *280*, 1055–1059.

Olsson, W. A. (1988), The effects of normal stress history on rock friction, in *Key Questions in Rock Mechanics: Proceedings of the 29th U.S. Symposium*, edited by P. A. Cundall, R. L. Sterling, and A. M. Starfield, pp. 111–117, A. A. Balkema, Brookfield, Vt.

Perfettini, H., and J. Schmittbuhl (2001), Periodic loading on a creeping fault: Implications for tides, *Geophys. Res. Lett.*, *28*(3), 435–438.

Perfettini, H., J. Schmittbuhl, J. R. Rice, and M. Cocco (2001), Frictional response induced by time-dependent fluctuations of the normal loading, *J. Geophys. Res.*, *106*(B7), 13,455–13,472.

Prakash, V. (1998), Frictional response of sliding interfaces subjected to time varying normal pressures, *J. Tribol.*, *120*, 97–102.

Prakash, V., and R. J. Clifton (1993), Time resolved dynamic friction measurements in pressure-shear, in *Experimental Techniques in the Dynamics of Deformable Solids*, edited by K. T. Ramesh, *AMD Ser.*, vol. 165, pp. 33–48, Appl. Mech. Div., Am. Soc. of Mech. Eng., New York.

Press, W. H., B. P. Flannery, S. A. Teukolsky, and W. T. Vetterling (1992), Integration of ordinary differential equations, in *Numerical Recipes in C: The Art of Scientific Computing*, 2nd ed., pp. 701–744, Cambridge Univ. Press, New York.

Ranjith, K., and J. R. Rice (2001), Slip dynamics at an interface between dissimilar materials, *J. Mech. Phys.*, *49*, 341–361.

Richardson, E., and C. Marone (1999), Effects of normal stress vibrations on frictional healing, *J. Geophys. Res.*, *104*, 28,859–28,878.

Ruina, A. L. (1983), Slip instability and state variable friction laws, *J. Geophys. Res.*, *88*, 10,359–10,370.

Saffer, D. M., K. M. Frye, C. Marone, and K. Mair (2001), Laboratory results indicating complex and potentially unstable frictional behavior of smectite clay, *Geophys. Res. Lett.*, *28*, 2297–2300.

Simões, F. M. F., and J. A. C. Martins (1998), Instability and ill-posedness in some friction problems, *Int. J. Eng. Sci.*, *36*, 1265–1293.

Sleep, N. H. (1997), Application of a unified rate and state friction theory to the mechanics of fault zones with strain localization, *J. Geophys. Res.*, *102*, 2875–2895.

Sleep, N. H., E. Richardson, and C. Marone (2000), Physics of friction and strain rate localization in simulated fault gouge, *J. Geophys. Res.*, *105*, 25,875–25,890.

Spudich, P., L. K. Steck, M. Hellweg, J. B. Fletcher, and L. M. Baker (1995), Transient stresses at Parkfield, California, pro-

duced by the *M* 7.4 Landers earthquake of June 28, 1992: Observations from the UPSAR dense seismograph array, *J. Geophys. Res.*, *100*(B1), 675–690.

Tolstoy, M., F. Vernon, J. Orcutt, and F. Wyatt (2002), Breathing of the seafloor: Tidal correlations of seismicity at axial volcano, *Geology*, *30*(6), 503–506.

Tworzydlo, W. W., and O. N. Hamzeh (1997), On the importance of normal vibrations in modeling of stick slip in rock sliding, *J. Geophys. Res.*, *102*, 15,091–15,103.

Vidale, J. E., D. C. Agnew, M. J. S. Johnson, and D. H. Oppenheimer (1998), Absence of earthquake correlation with Earth tides: An indication of high preseismic fault stress rate, *J. Geophys. Res.*, *103*, 24,567–24,572.

Wang, W., and C. H. Scholz (1994), Micromechanics of the velocity and normal stress dependence of rock friction, *Pure Appl. Geophys.*, *143*, 303–315.

Wilcock, W. S. (2001), Tidal triggering of microearthquakes on the Juan de Fuca Ridge, *Geophys. Res. Lett.*, *28*(20), 3999–4002.

Wyss, M., and S. Wiemer (2000), Change in the probability for earthquakes in Southern California due to the Landers magnitude 7.3 earthquake, *Science*, *290*, 1334–1338.